Electropolymerized Poly(1,10-phenanthroline)-Iodine Complex as a High-Capacity and Stable Cathode for Zinc-Iodine Batteries

Shuling Liu*, Rui Su, Qiangqiang Shi, Shaoyan Huang, Miaomiao Dong, Yu Cao

Department of Chemistry and Chemical Engineering, Shaanxi Collaborative Innovation Center of Industrial Auxiliary Chemistry & Technology, Key Laboratory of Auxiliary Chemistry and Technology for Chemical Industry, Ministry of Education, The Youth Innovation Team of Shaanxi Universities, Shaanxi University of Science and Technology, Xi'an, Shaanxi 710021, P. R. China

*Corresponding author.

E-mail address: liushuling@sust.edu.cn

Experimental

Chemicals

The following reagents were used without further purifications. ZnI_2 (AR, 99.5%), 1,10-phenanthroline (Phen, AR, 99.0%), concentrated sulfuric acid (H_2SO_4, AR, 98.0%), carbon paper (HCP020N) and doubly distilled water.

Preparation of PPhen-I/CP-1, PPhen-I/CP-2, and PPhen-I/CP-3

The PPhen-I/CP was fabricated through electrodeposition using a CP substrate in a three-electrode setup. The electrodeposition electrolyte consisted of 15 mmol Phen and 30 mmol ZnI_2 in a 0.5 M sulfuric acid solution. The mixture was stirred at room temperature for approximately 10 minutes to achieve homogeneous distribution. The prepared CP, serving as the working electrode, was immersed in the electrolyte. A constant potential of 1.6 V_{SCE} was applied at room temperature for 1000s. The electrodes with the highest discharge capacity were obtained by optimizing the electrochemical deposition parameters such as electrolyte concentration, current density and deposition time. The electrolyte concentration was varied by varying different molar ratios of Phen and ZnI_2 (Phen: ZnI_2=1:4, 1:2, 2:1) labeled as PPhen-I/CP-1, PPhen-I/CP-2, PPhen-I/CP-3, respectively. The sample was then thoroughly rinsed with water and dried at 60 ℃ for 12 h.

Material characterization

The crystalline phase of the samples was measured by X-ray diffractometer (Bruker

D8 Advance, Bragg-Brentano geometrical configuration) at a temperature of 25°C, a voltage of 40 kV, and a current density of 30 mA. The diffraction angle scanning range was 2θ = 5-80°, and X-ray diffractograms were obtained by placing the samples (thin films) directly on the sample holder. The X-ray diffraction data were analyzed using MDI JADE software. The microstructure and morphology of the samples were observed using a Hitachi S-4800 scanning electron microscope (SEM) equipped with an energy-dispersive X-ray spectroscopy (EDS) analysis unit . A hybrid lens was used to form an x-ray photoelectron spectrum with a spot size of 700 × 400 mm^2. The samples were kept in air before entering the XPS instrument chamber at room temperature and under ultra-high vacuum conditions. All high-resolution XPS spectra were calibrated against the c1s peak at 284.8 eV when analyzed using the CasaXPS software. Titration analysis was performed using ultraviolet-visible spectrophotometry. First, a standard curve of absorbance (A) versus concentration (C) for I_3^- was established at 350 nm (A = kC + b) using standard solutions of known concentration. Subsequently, the adsorbent was immersed in the I_3^- solution for reaction. At different time points, samples were taken, and the absorbance (A_t) of the supernatant was measured. The concentration (C_t) in the solution was then calculated based on the standard curve. The UV-vis measurements were carried out using a quartz cuvette with a path length of 1 cm, and the sample concentration was adjusted to ensure an absorbance within the linear range.

Electrochemical characterization

The electrodes were prepared as follows: The electrode preparation method for

electrochemical characterization is as follows: First, the deposited samples were cut into 12 mm discs. Subsequently, the cells were assembled using PPhen-I/CP-1, PPhen-I/CP-2, PPhen-I/CP-3, PPhen/CP, and ZnI_2/CP as the cathodes, a metallic zinc anode, and a 2 M $ZnSO_4$ aqueous electrolyte solution, respectively. Constant-current charge-discharge (GCD), cyclic voltammetry (CV), and electrochemical impedance spectroscopy (EIS) tests were conducted on an electrochemical workstation (CHI660E). Rate performance and stability tests were performed at room temperature using a battery tester (Neware BTS 7.6x). Cyclic voltammetry was performed over a voltage range of 0.4-1.6 V. Electrochemical impedance spectroscopy was conducted at frequencies ranging from 10^5 to 0.01 Hz with an AC amplitude of 5 mV. All electrochemical measurements were conducted at room temperature.

Calculation of Zn^{2+} diffusion coefficients through CV curves (Randles-Sevcik Method): The diffusion coefficient value (D) can be calculated from the following formula[1]:

$$i_p = (2.69 \times 10^5)\, n^{3/2} A D^{1/2} C v^{1/2} \qquad (1)$$

where i_p is the peak current density (A g^{-1}), n is the number of electrons per molecule during the intercalation, A is the surface area of the cathode (cm^2), C is the concentration of Zn^{2+} in the electrode (mol cm^{-3}), and v is the corresponding scan rate (V s^{-1}).

Supplementary Figures

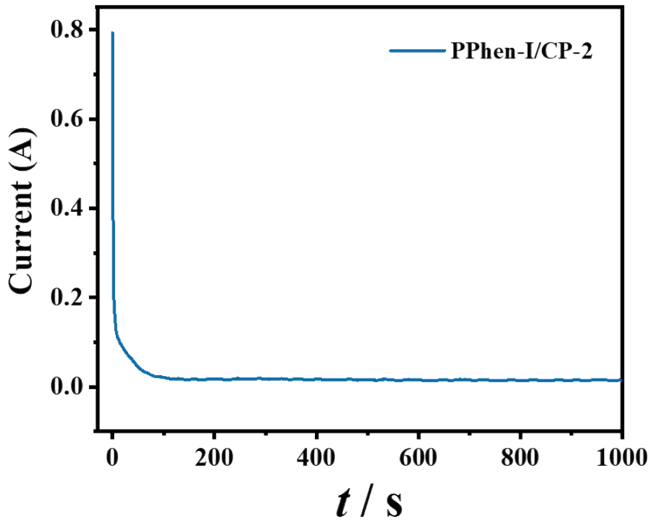

Fig S1. Under a constant potential of 1.6 V, the E-t deposition curves of 2M H_2SO_4 aqueous solution with PPhen-I/CP-2

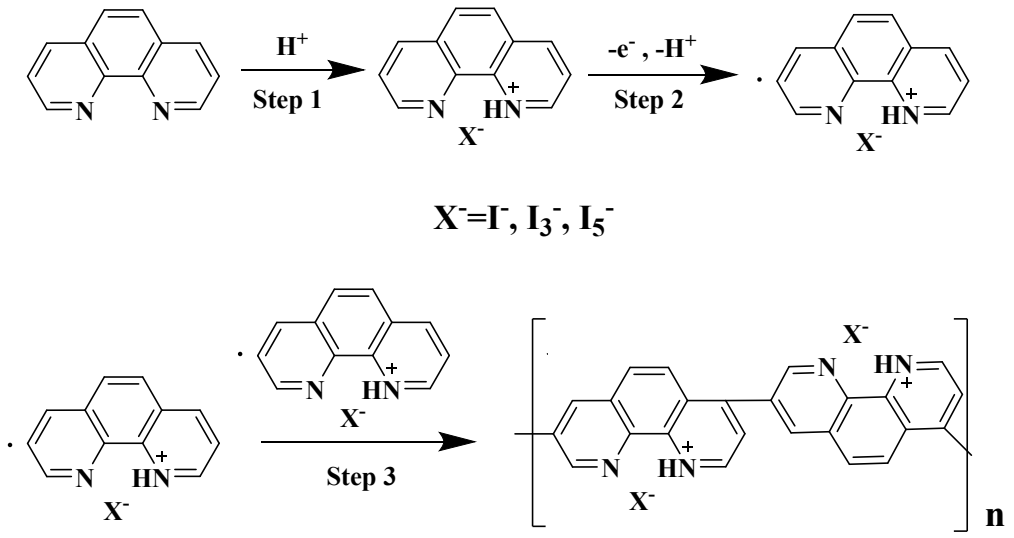

Fig S2. Proposed mechanism for electropolymerization of Phen and iodide.

Iodine was loaded onto PPhen by the constant voltage method (1.6 V) in acidic aqueous solution. Based on previous studies on the electrografting and electropolymerization of Phen[2–4], we propose the following mechanism for iodine-loaded PPhen (Fig S2): Phen behaves as a weak base (pKa = 4.9-5.09)[5,6], which is protonated in an acidic aqueous environment (Step 1). And iodide ions are present in the polymer matrix as negatively charged counterbalance ions. Electrooxidation of a benzene ring occurs at the position of the weakest hydrogen bond, a process that involves the transfer of an electron and a proton (step 2). Polymerization is initiated by the presence of Phen cationic radicals in the vicinity, and covalent bonds are formed between the carbon atoms of the two Phen molecules (step 3). During the electropolymerization process, I_2 is converted to polyiodides such as I_3^- or I_5^- in the presence of excess I^- , enabling the effective incorporation of iodide species (I^-, I_3^- or I_5^-) into the polymer matrix.

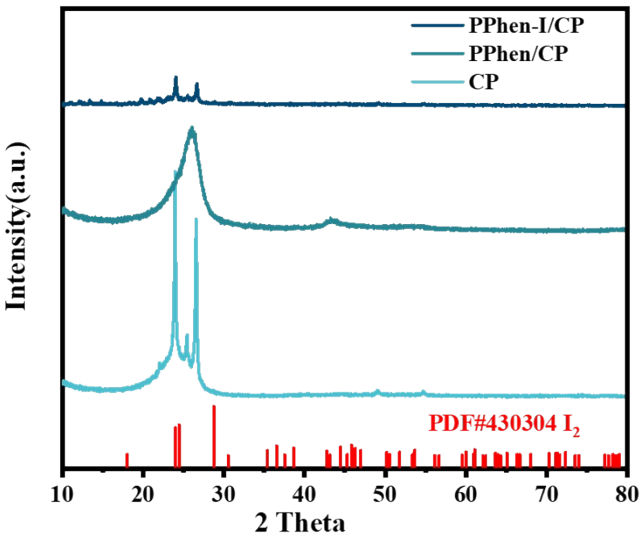

Fig S3. XRD patterns of PPhen/CP, PPhen-I/CP-2, and pure I_2.

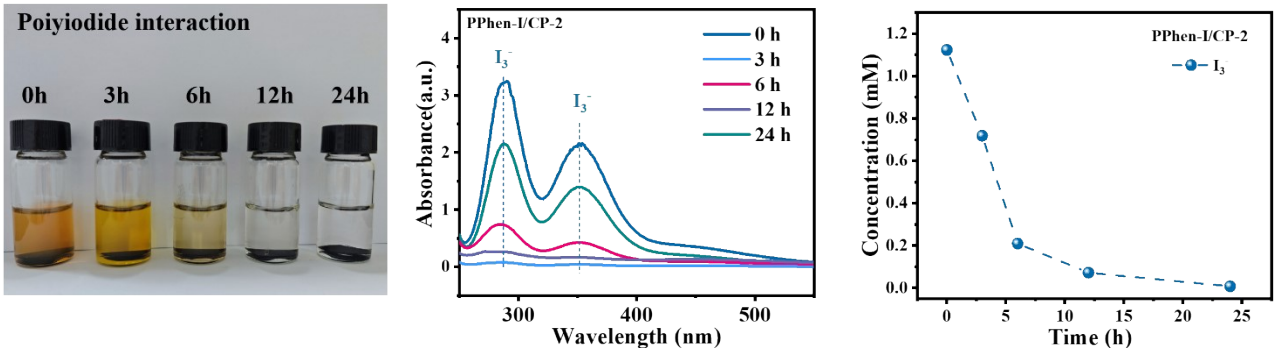

Fig S4. (a) Photographs of polyiodide-containing solution after incubation with PPhen/CP at different time intervals. (b) UV-vis spectra of the polyiodide solution with PPhen/CP. (c) Quantitative analysis of I_3^- concentrationinsolution by UV-vis absorption.

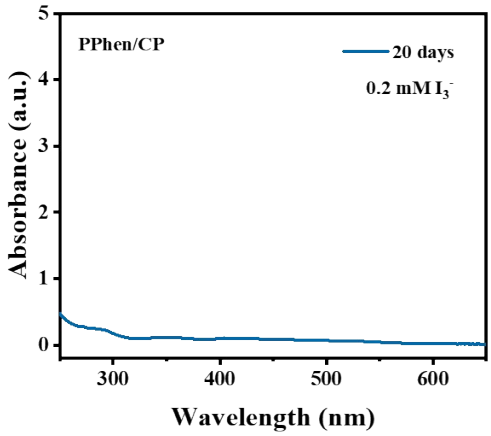

Fig S5. UV-vis spectra and concentration of the polyiodide solution after 20 days (soaked with PPhen/CP)

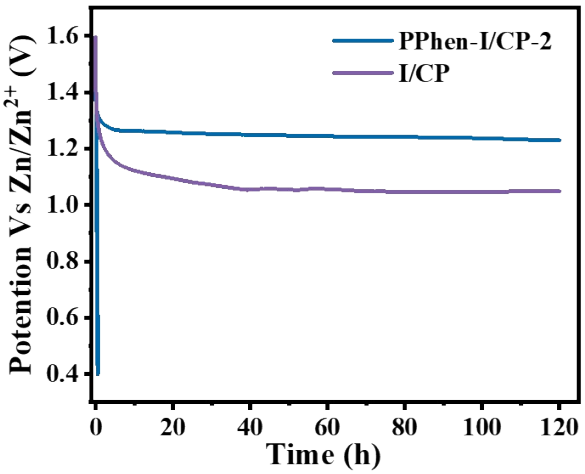

Fig S6. self-discharge test of PPhen-I/CP-2 and I/CP cathode.

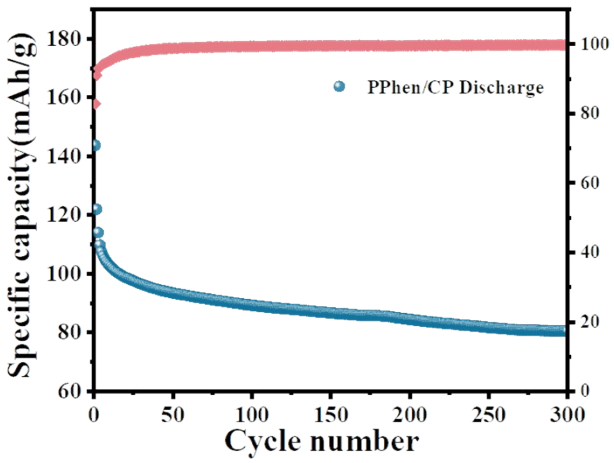

Fig S7. Cycling performance of PPhen/CP electrode at at 0.2 A g^{-1}

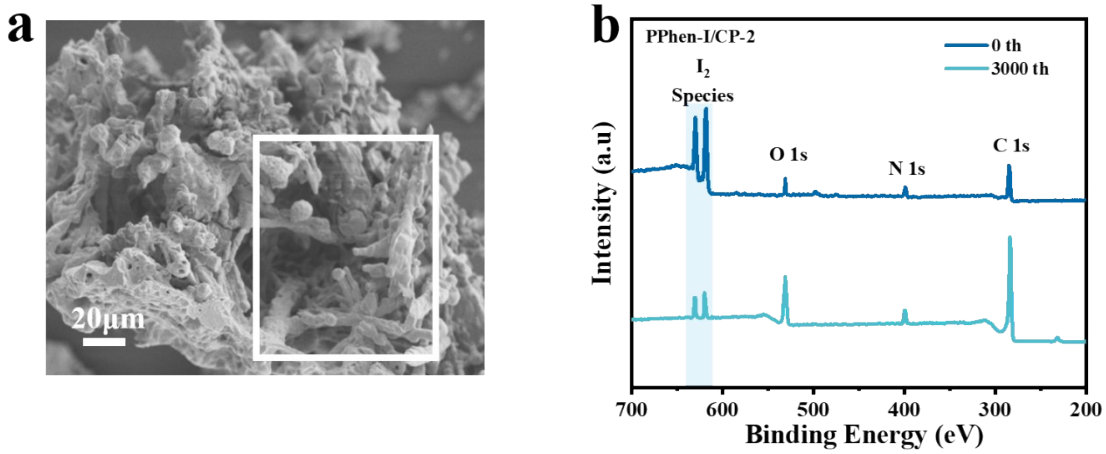

Fig S8. (a) SEM and (b) XPS spectra of the PPhen-I/CP-2 cathode after 3,000 cycles at 2 A g^{-1}

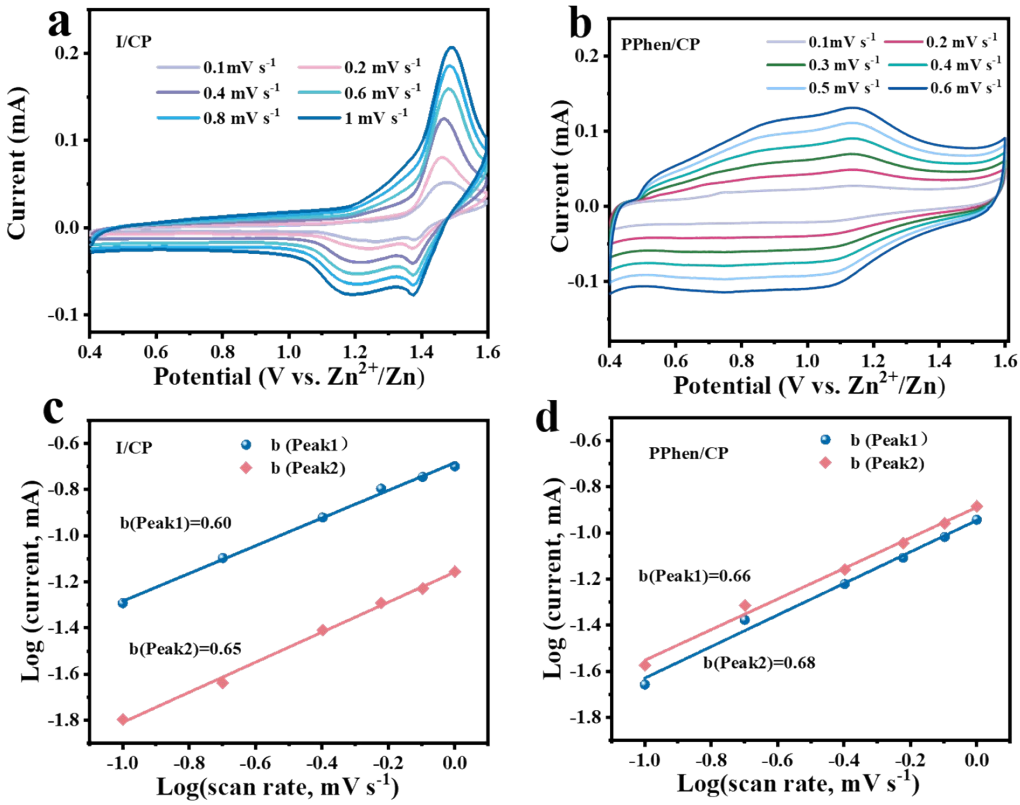

Fig S9. CV curves of (a) I/CP and b) PPhen/CP cathodes at different scan rates. The relationships between peak current density and scan rate in ZIBs with c) I/CP and d) PPhen/CP cathodes.

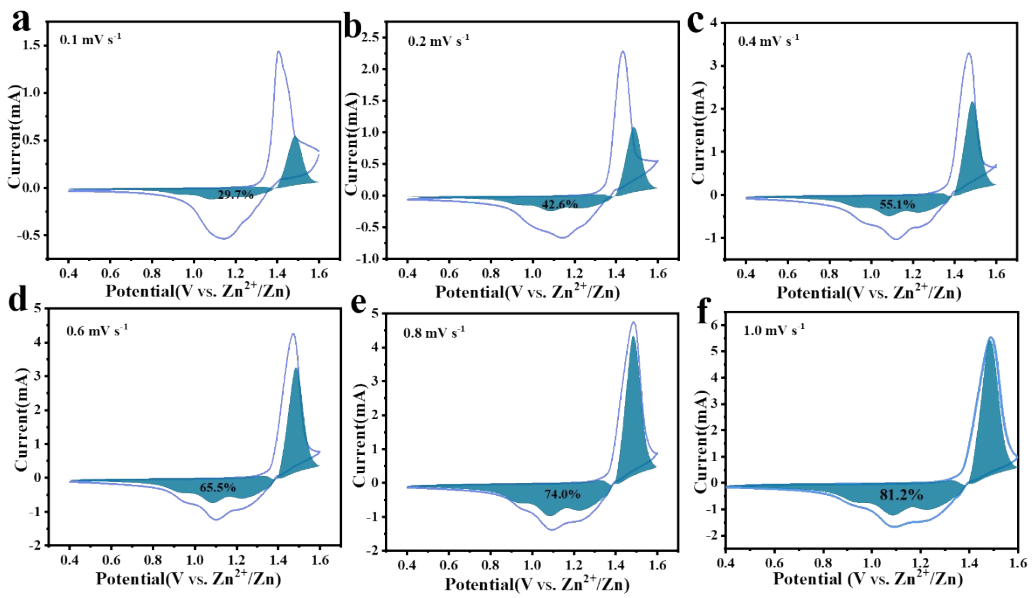

Fig S10. The estimated capacitive contributions of the PPhen-I/CP-2 cathode at different scan rates of (a) 0.1, (b) 0.2, (c) 0.4, (d) 0.6, (e) 0.8, and (f) 1 mV s^{-1}.

	R_1	CPE1-T	CPE1-P	R_{ct}	W1-R	W1-T	W1-P
PPhen-I/CP-2	68.75	0.00002547	0.8768	41.24	81.23	0.459	0.3292
I/CP	1.966	0.00005103	0.7800	70.85	361.6	126.5	0.5153
PPhen/CP	101.4	0.000043106	0.8323	104.7	569.1	453	0.3777

Table S1. The fitting results of the Nyquist plots of PPhen-I/CP-2, I/CP, PPhen/CP.

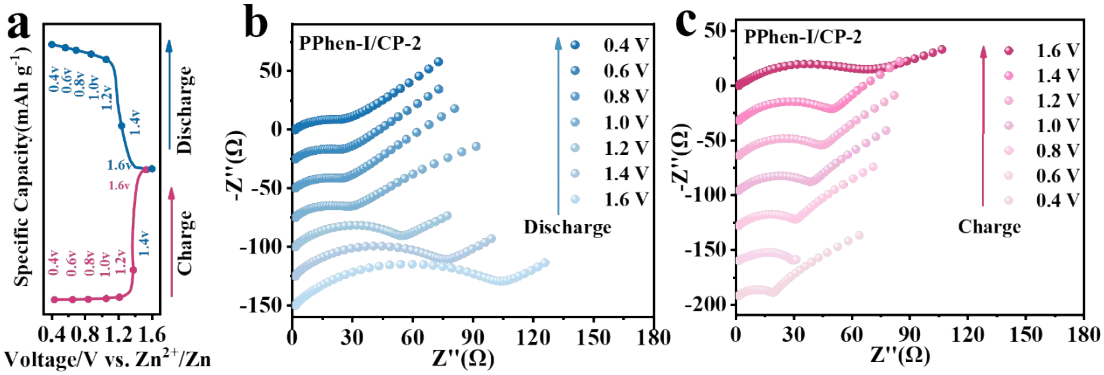

Fig S11. (a) In situ EIS spectra of the PPhen-I/CP-2 cathode collected at various potentials during the b) discharge and c) charge process.

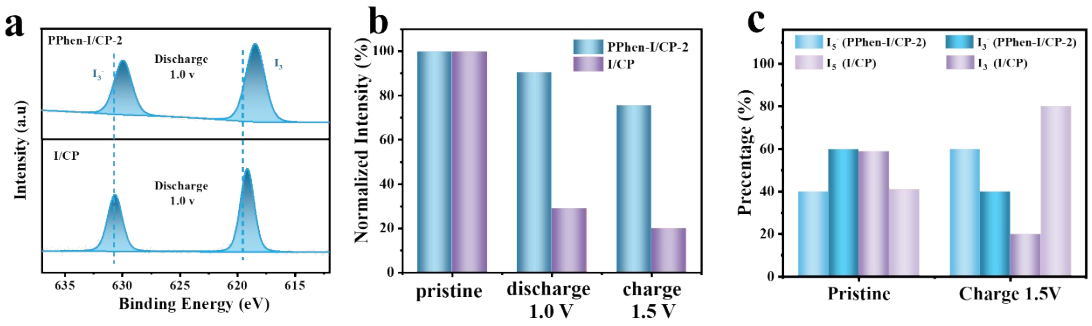

Fig S12. (a) XPS of I_3^- of I/CP and PPhen-I/CP-2 at a discharge state of 1.0V. (b) Calculate the total iodine content in I/CP and PPhen-I/CP-2 at different redox charged and discharged states. (c) Calculated I content from XPS I3d at corresponding states.

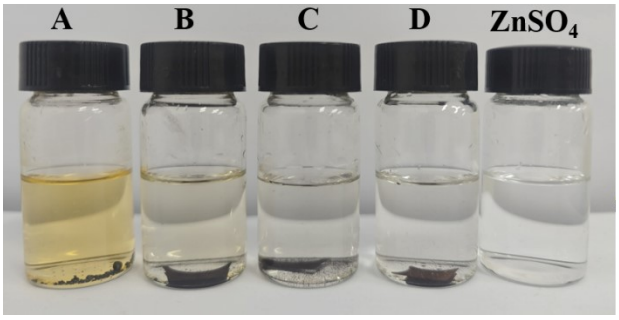

Fig S13. I_2, PPhen-I/CP-1 (A), PPhen-I/CP-2 (B), and PPhen-I/CP-3 (C), soaked for 1 months in 2 M ZnSO4 electrolyte.

Electrode material	Current density	Specific capacity	Ref.
PPy/I	0.1 A g^{-1}	201 mAh g^{-1}	[7]
	2 A g^{-1}	123 mAh g^{-1}	
Zn//PPy-I	0.05 A g^{-1}	145 mAh g^{-1}	[8]
	0.5 A g^{-1}	190 mAh g^{-1}	
MPC/I	1 A g^{-1}	107 mAh g^{-1}	[9]
	0.1 A g^{-1}	137 mAh g^{-1}	
N-LPC	0.1 A g^{-1}	127 mAh g^{-1}	[10]
PANI	1.5 A g^{-1}	160 mAh g^{-1}	[11]
VIPC-I	0.2 A g^{-1}	146.9 mAh g^{-1}	[12]
	3 A g^{-1}	119.0 mAh g^{-1}	
I_2-Nb_2CT_X MXene	1 A g^{-1}	205 mAh g^{-1}	[13]
Bpd-COC	2 A g^{-1}	110.8 mAh g^{-1}	[14]
NCCs/I	0.2 A g^{-1}	222 mAh g^{-1}	[15]
PPhen-I/CP-2	0.2 A g^{-1}	270 mAh g^{-1}	This work
	2 A g^{-1}	160 mAh g^{-1}	This work

Table S2. Comparison of host materials in zinc-iodine battery.

Electrode material	Energy density	Power density	Ref.
PPy/I	246 Wh kg^{-1}	123 W kg^{-1}	[7]
NCCs/I	282 Wh kg^{-1}	_	[15]
I_2-Nb_2CT_X MXene	259.3 Wh kg^{-1}	23 505 W kg^{-1}	[13]
Zn||KB-I_2	189.5 Wh kg^{-1}	_	[16]
OHPCF-0.5/I_2	210.5 Wh kg^{-1}	297.2 W kg^{-1}	[17]
I_2-HPCM-NP	165.6 Wh kg^{-1}	40.4 W kg^{-1}	[18]
PPhen-I/CP-2	289.1913 Wh kg^{-1}	696.555 Wh kg^{-1}	This work

Table S3. Comparison of key performance metrics for zinc-iodine batteries.

Refence

1 Z. Zhou, J. Tong, X. Zou, Y. Wang, Y. Bai, Y. Yang, Y. Li, C. Wang and S. Liu, *J. Mater. Chem. A*, 2024, **12**, 10923–10931.

2 C. Wang, Z. Zhou, Q. Tian, X. Cao, Y. Wu, S. Liu and J. Wang, *Chemical Engineering Journal*, 2022, **433**, 134483.

3 G. Shul, M. Weissmann and D. Bélanger, *Langmuir*, 2014, **30**, 6612–6621.

4 G. Shul, M. Weissmann and D. Bélanger, *Electrochimica Acta*, 2015, **162**, 146–155.

5 C. V. Krishnan, C. Creutz, H. A. Schwarz and N. Sutin, *J. Am. Chem. Soc.*, 1983, **105**, 5617–5623.

6 F. Najóczki, M. Szabó, N. Lihi, A. Udvardy and I. Fábián, *Molecules*, 2021, **26**, 3632.

7 L. Zhou, N. Wang, Y. Chang, S. Zhu, Y. Zhang, W. Hou, Y. Zhao and G. Han, *Journal of Energy Storage*, 2024, **88**, 111538.

8 X. Wang, Y. Chang, H. Song, W. Hou, Y. Zhang, Y. Li, G. Han and Y. Xiao, *Journal of Electroanalytical Chemistry*, 2022, **912**, 116232.

9 Y. Hou, F. Kong, Z. Wang, M. Ren, C. Qiao, W. Liu, J. Yao, C. Zhang and H. Zhao, *Journal of Colloid and Interface Science*, 2023, **629**, 279–287.

10 Y. Ji, J. Xu, Z. Wang, M. Ren, Y. Wu, W. Liu, J. Yao, C. Zhang and H. Zhao, *Journal of Electroanalytical Chemistry*, 2023, **931**, 117188.

11 X. Zeng, X. Meng, W. Jiang, J. Liu, M. Ling, L. Yan and C. Liang, *ACS Sustainable Chem. Eng.*, 2020, **8**, 14280–14285.

12 L. Qiu, L. Zhang, Z. Liang, S. Liu, Y. Zhang, S. Gao, Y. Zhang, E. Debroye, J. Hofkens, J. Huang and F. Lai, *Chemical Engineering Journal*, 2025, **514**, 162992.

13 X. Li, N. Li, Z. Huang, Z. Chen, G. Liang, Q. Yang, M. Li, Y. Zhao, L. Ma, B. Dong, Q. Huang, J. Fan and C. Zhi, *Advanced Materials*, 2021, **33**, 2006897.

14 Z. Zhu, D. Luo, L. Wei, J. Chen, T. Jia, X. Chi and X. Guo, *Energy Storage Materials*, 2025, **75**, 103994.

15 W. Liu, P. Liu, Y. Lyu, J. Wen, R. Hao, J. Zheng, K. Liu, Y.-J. Li and S. Wang, *ACS Appl. Mater. Interfaces*, 2022, **14**, 8955–8962.

16 S.-J. Zhang, J. Hao, H. Wu, Q. Chen, Y. Hu, X. Zhao and S.-Z. Qiao, *J. Am. Chem. Soc.*, 2025, **147**, 16350–16361.

17 L. Wei, X. Zhang, X. Li, C. Chen, D. Yu and G. Zhao, *Journal of Electroanalytical Chemistry*, 2024, **967**, 118452.

18 K. Lu, Z. Hu, J. Ma, H. Ma, L. Dai and J. Zhang, *Nat Commun*, 2017, **8**, 527.